

Modeling of Braided Pneumatic Actuators for Robotic Control

Robb W. Colbrunn, Gabriel M. Nelson, Roger D. Quinn

Case Western Reserve University
Cleveland, Ohio 44106

Abstract

Braided Pneumatic Actuators exhibit non-linear force-length properties grossly similar to muscle, and have a high strength-to-weight ratio. These properties make them desirable for legged robots. This work emphasizes understanding the actuator properties for later use in simulation and control of legged robots. Static and dynamic mathematical models for the actuators are reported and verified through testing and simulation. In addition, a dynamic air flow model modulated by a solenoid valve was developed to provide modular actuation subroutines for simulation.

1. Introduction

The many successful and capable legged animals provide evidence that legs are advantageous for moving vehicles over irregular terrain. However, there are many challenging problems that first must be solved before legged robots can be nearly as successful as their biological counterparts. One of these is the implementation of actuators that rival the desirable properties of muscle such as high strength to weight, structural flexibility and tunable passive stiffness. The Braided Pneumatic Actuator (BPA), otherwise known as a Rubbertuator [6] or McKibben Artificial Muscle [3], is one such candidate that meets these requirements. They have been shown to have gross force-length properties similar to animal muscle [7] and a BPA weighing less than one pound can lift 250lbs at more than 20% strain. The BPA was patented by Gaylord [5] and used by McKibben [12] in orthotic devices in the late 1950's.

A simple BPA (Fig. 1) can be constructed by inserting a latex tube inside a braided tube such as flexible electrical conduit. Plugs are inserted into each end of the latex tube and clamps are placed over the ends, fastening the tubes to the plugs. A hole is drilled in one end-plug and an air hose is inserted into it. When the latex tube is inflated with compressed air, it forces the braided tube to expand circumferentially, which causes it to shrink in length. It is typically a tension actuator. The cylindrical center section of the actuators in Figure 1 are $\frac{1}{4}$ " x 3.85" long when fully stretched. Shadow Robot Company of London, England manufactured the actuators used in this work [14].

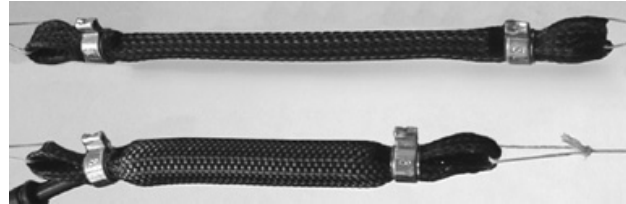


Figure 1. Inflated and Deflated BPA

2. Static Model

The formulation described in this section follows the work of Chou and Hannaford [3] in modeling BPA. A similar formulation will be used, but the final form of the equations will better suit our needs of modeling and controlling them. Next, these equations will be used to derive further relationships between force, pressure, length, and stiffness. These relationships will then be verified and fine-tuned with empirical data.

A BPA is modeled as a cylinder and the wall thickness is assumed to be zero. The dimensions of this cylinder are the length L and diameter D . Assuming inextensibility of the mesh material, the geometric constants of the system are the thread length b and the number of turns for a single thread n . The final dimension used for this formulation is the interweave angle θ , which is the angle between the thread and the long axis of the cylinder. The interweave angle changes as the length of the actuator changes. The relationship between these parameters is shown in Figure 2.

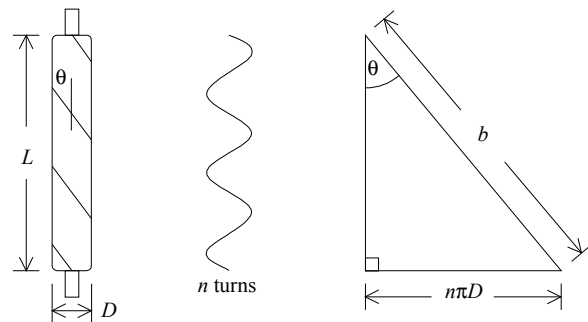


Figure 2. Geometric model of BPA [3].

Using this model, Chou and Hannaford [3] derived the following equation for actuator force F as a function of the cylindrical parameters and the internal gage pressure P_g .

$$F = \frac{P_g b^2 (3 \cos^2 \theta - 1)}{4\pi n^2} \quad (1)$$

It is difficult to sense the interweave angle during operation of the actuator. Expressing the equations in terms of force, pressure, and length will be more useful for control purposes. Recall the triangle from Figure 2 and note that a relationship can be expressed between θ , L , and b .

$$\cos \theta = \frac{L}{b} \quad (2)$$

Substituting this relationship into Eq. (1),

$$F = \frac{P_g b^2}{4\pi n^2} \left(\frac{3L^2}{b^2} - 1 \right) \quad (3)$$

This is the same relationship reported by Tondu et al. [15] with the end effect parameter set to unity. BPA exhibit the properties of a variable stiffness spring. Joint angle is a relatively easy quantity to sense. However, stiffness is not. Therefore a model of actuator stiffness was developed. Stiffness, k , is simply a derivative of force with respect to length.

$$k = \frac{dF}{dL} \quad (4)$$

Differentiating (3) with respect to L ,

$$k = \frac{b^2}{4\pi n^2} \left(\frac{3L^2}{b^2} - 1 \right) \frac{dP_g}{dL} + \frac{3P_g L}{2\pi n^2} \quad (5)$$

The first term (dP_g/dL) is the most difficult to formulate. When the valves are closed, the pressure changes proportionally with volume, V , according to gas laws. When the valves are opened, this relationship is even more difficult to model. However, if the external volume to the actuator (e.g. in the inlet hose) is roughly the same or more than the maximum internal actuator volume, then the total volume is enough to cause the pressure change to remain minimal through the actuator's range of motion. In this case we can assume:

$$\frac{dP_g}{dL} \approx 0 \quad (6)$$

Actuator stiffness is now given by:

$$k = \frac{3P_g L}{2\pi n^2} \quad (7)$$

Or solving (3) for P_g and substituting the result into (7),

$$k = \frac{6F}{\left(3L - \frac{b^2}{L} \right)} \quad (8)$$

Figure 3 is a plot of theoretical actuator force and stiffness as a function of internal pressure (Eqs. (3) and (7)) for the range from 35 to 95 psi. Force is a nonlinear function of length, tending to zero at maximum contraction, and

stiffness is a linearly increasing function of length and pressure.

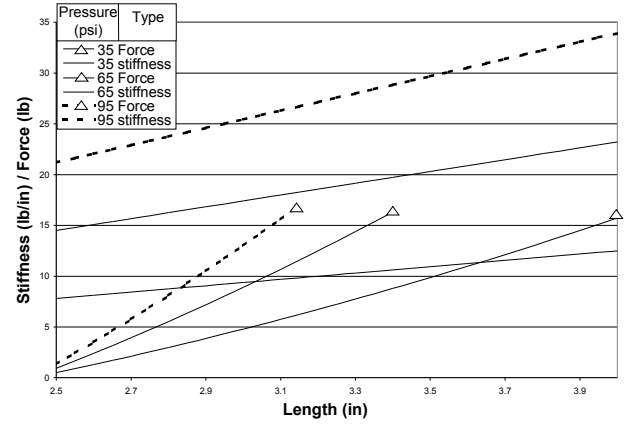


Figure 3. Theoretical pressure, length, force, stiffness relationship for the BPA shown in Figure 1.

2.1 Static Model Verification

Chou and Hannaford [3], using constant pressure testing, have verified the model of force as a function of pressure and length (1). In the control of the robotic leg described in our other paper in this volume, internal air mass is the variable being controlled instead of pressure. Therefore, we tested a system with constant air mass. The actuator was inflated to some nominal pressure and the valve was then closed. A mass M was suspended from the BPA and was increased in 1 lb increments to a maximum of 15 lbs and then decreased to zero in 1 lb increments. Four tests were performed, each at a different nominal pressure, and the results are shown in Fig. 4.

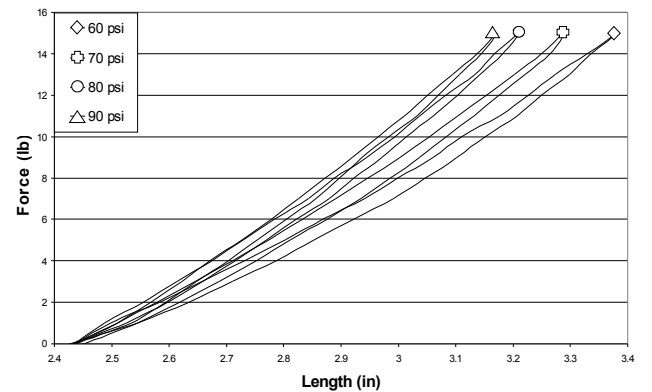


Figure 4. Force vs. Length for a Braided Pneumatic Actuator with Constant Internal Mass of Air.

The force output of a BPA is a non-linear function of length. The closed curves in Figure 4 also show the hysteresis of the actuators, which is a by-product of the Coulomb friction between the bladder and the mesh [3].

Figure 5 is a comparison of the predicted and measured force-length properties at two pressures.

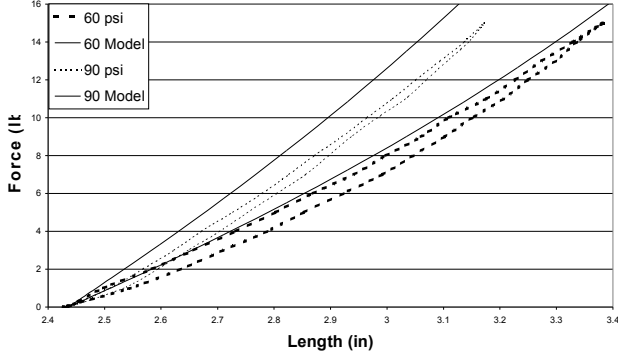


Figure 5. Plot of predicted and experimental force output vs. length at the nominal pressures of 60 and 90 psi.

The model does not predict the hysteresis nor does it perfectly match the experimental data. The model predicts a higher force output than what was measured. Our goal is to develop a simple model that is adequate for control. Therefore, a correction factor that we call an effectiveness term is introduced. Effectiveness is the measure of what percentage the actual force is to the predicted. Figure 5 also suggests that effectiveness is a function of pressure:

$$F_{act} = Eff(P_g) \cdot F_{theoretical} \quad (9)$$

Effectiveness was determined for each nominal pressure, and a relationship for effectiveness as a function of pressure was created. After applying the effectiveness function to the model, the experimental and theoretical data sets were compared again (Figure 6) and the model is found to be representative of the experimental results.

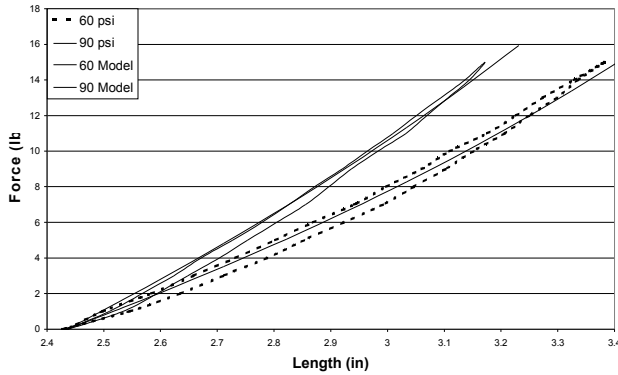


Figure 6. Force vs. Length comparison of experimental and theoretical Results including effectiveness term.

The final additions to the model are the end effects, which are changes in force output at the length limits of an actuator. When the actuator is at its maximum length L_{max}

any increase in length would cause the braids to stretch. Because the stiffness of the braiding material is very high compared to the stiffness of the actuator, the long end effect can be modeled as a spring of very high stiffness.

A BPA of this design that is attached using tendons can only pull. The model (3) predicts that if the length is less than the maximum contracted length, then the actuator will push. The short-end model causes the force output to be zero if the length is less than the minimum length, L_{min} . Incorporating the effectiveness and the end effects into (3) yields:

$$F = \begin{cases} \frac{P_g b^2}{4\pi n^2} \left(\frac{3L^2}{b^2} - 1 \right) \cdot Eff(P_g) + F_{max\ limit} & \text{if}(L > L_{min}) \\ 0 & \text{if}(L < L_{min}) \end{cases} \quad (10)$$

$$\text{where } F_{max\ limit} = \begin{cases} K_{braid}(L - L_{max}) & \text{if}(L > L_{max}) \\ 0 & \text{if}(L < L_{max}) \end{cases} \quad (11)$$

and K_{braid} = Braid material stiffness

Equation (10) is the static model for a BPA. This model ignores bladder thickness, friction-induced hysteresis, and non-linear elastic energy storage of the bladder. Klute and Hannaford [8] have developed a more accurate model considering these factors, but the cost of the more accurate model is more complex equations. This model is adequate and yet simple enough that it is suitable for dynamic simulations and control.

3. Dynamic Model

Our dynamic model of a BPA consists of a spring, viscous damper, and Coulomb friction all in parallel. The spring has a nonlinear force-length relationship given by (10). The viscous damper models the viscous effects of the fluid flow losses in the system. Coulomb friction models the losses due to the sliding contact between the mesh and bladder.

$$F = \begin{cases} \frac{P_g b^2}{4\pi n^2} \left(\frac{3L^2}{b^2} - 1 \right) \cdot Eff(P_g) + F_{max\ limit} + c \cdot v \pm Q \cdot k & \text{if}(L > L_{min}) \\ 0 & \text{if}(L < L_{min}) \end{cases} \quad (12)$$

$$k = \frac{\left(\frac{P_g b^2}{4\pi n^2} \left(\frac{3L^2}{b^2} - 1 \right) \cdot Eff(P_g) \right) - F_{min}}{L - L_{min}} \quad (13)$$

where c = viscous damping constant, v = actuator tip velocity, k = linearized actuator stiffness, and $Q = \frac{\mu N}{k}$.

Equation (13) is a linearized stiffness equation ($\Delta F/\Delta L$). F_{min} is the force output at L_{min} . Which, according to (1), is always null. Viscous damping of the mesh material was

also added through its inclusion in the $F_{max\ limit}$ equation (11).

$$F_{max\ limit} = \begin{cases} K_{braid}(L - L_{max}) + C_{braid}v & \text{if}(L > L_{max}) \\ 0 & \text{if}(L < L_{max}) \end{cases} \quad (14)$$

where C_{braid} = Braid viscous damping constant. The damping constants were determined experimentally.

3.1 Simulation

The purpose of the simulation (Fig. 7) was not only to verify the dynamic model of a BPA, but also to create a model of a BPA working in conjunction with a solenoid valve. The simulation has four state variables: length L , velocity \dot{L} , pressure P , and air mass m . To determine the next system state, the equations of motion (EOM) were integrated using the Runge-Kutta algorithm. The valve state is calculated at each time step according to the system state or the time.

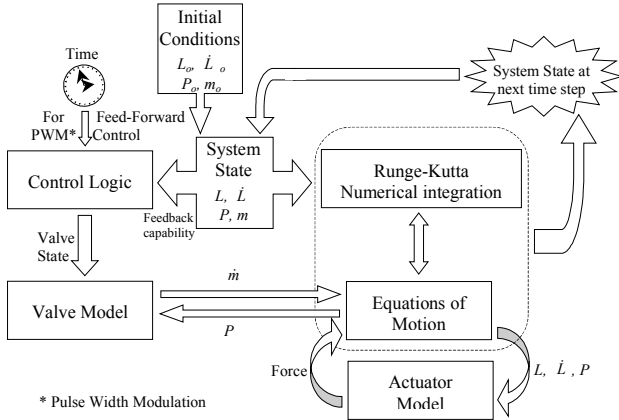


Figure 7. Simulation block diagram.

3.1.1 Equations of Motion

A mass-spring-damper system was controlled in the simulation where the spring force is a function of the mass of air in the actuator. There are two different EOM in this system. One equation defines the movement of the suspended mass M , and the other defines the movement of the air. The first EOM was formulated for the motion of M as a function of actuator and gravitational forces. Applying Newtons second law

$$\sum F = -F_{actuator} + Mg = M\ddot{L} \quad (15)$$

Solving for \ddot{L} ,

$$\ddot{L} = g - \frac{F_{actuator}}{M} \quad (16)$$

The second EOM is a state relationship for the air in the system [9]. The first step is to take the time derivative of the standard mass-volume-density relationship.

$$\frac{d}{dt} \left(\rho = \frac{m}{V} \right) \rightarrow \dot{\rho} = \frac{\dot{m}}{V} - m \frac{\dot{V}}{V^2} \rightarrow \dot{\rho} = \frac{\dot{m}}{V} - \rho \frac{\dot{V}}{V} \quad (17)$$

where ρ = density, V = volume, m = air mass. The next step is to take a time derivative of the constant pressure-density relationship. This is based on an adiabatic flow assumption.

$$\frac{d}{dt} (P\rho^{-\gamma} = \text{constant}) \rightarrow \frac{\dot{P}}{\rho^{\gamma}} - \frac{\gamma P \dot{\rho}}{\rho^{\gamma+1}} = 0 \rightarrow \dot{P}\rho = \gamma P \dot{\rho} \quad (18)$$

where P = absolute pressure and the specific heat ratio is assumed to be $\gamma = 1.4$. Substituting (17) into (18),

$$\dot{P} = \gamma \frac{P}{\rho} \left(\frac{\dot{m}}{V} - \rho \frac{\dot{V}}{V} \right) \rightarrow \dot{P} = \gamma P \left(\frac{\dot{m}}{m} - \frac{\dot{V}}{V} \right) \quad (19)$$

The volume flow rate is the time derivative of the geometry formulated volume equation [4].

$$\dot{V} = \frac{(b^2 - 3L^2)}{4\pi n^2} \dot{L} \quad (20)$$

Note that V is a summation of the actuator volume and the external volume (i.e. hoses), not just the actuator volume. The two equations of motion, (16) and (19), provide the relationships necessary for numerical integration in the simulation. To complete (19) the valve model needs to be formulated.

3.2 Valve Model

The mass flow rate through a valve can be expressed by the following equation [9] [16].

$$\dot{m} = \frac{A_p P_{up} C_q C_m}{\sqrt{T_{am}}} \quad (21)$$

where A_p = air passage area of solenoid valve, P_{up} = upstream air pressure (absolute), C_q = flow rate coefficient, C_m = flow rate parameter, T_{am} = temperature of upstream air.

C_q is an empirically determined efficiency term. It can be expressed as,

$$C_q = \frac{\dot{m}_{measured}}{\dot{m}_{calculated\ with\ C_q = 1}} \quad (22)$$

C_m changes depending on whether the flow through the valve is choked or not. It is defined by the following;

$$C_m = \begin{cases} \sqrt{\frac{\gamma}{R} \left(\frac{2}{\gamma+1} \right)^{\frac{\gamma+1}{\gamma-1}}} & \frac{P_{down}}{P_{up}} \leq 0.528 \text{ (choked)} \\ \sqrt{\frac{2\gamma}{R(\gamma-1)} \left[\left(\frac{P_{down}}{P_{up}} \right)^{\frac{2}{\gamma}} - \left(\frac{P_{down}}{P_{up}} \right)^{\frac{\gamma+1}{\gamma}} \right]} & \frac{P_{down}}{P_{up}} > 0.528 \text{ (not choked)} \end{cases} \quad (23)$$

where P_{down} = downstream air pressure (absolute) and $R = 53.34 \frac{ft \ lbf}{lbm \ ^\circ R}$ is the air constant.

The above model was used, and the empirically determined constants were evaluated [10]. An eight-channel three-way valve manufactured by Matrix was used in the verification of the dynamic actuator model. Due to the complex geometry of the solenoid valves, the A_p term was lumped with the C_q term and backed out of the pressure-flowrate plot given in valve literature specifications. $A_p C_q$ was found to be $1.8 \times 10^{-5} \text{ ft}^2$ for these valves.

3.3 Dynamic Model Verification

The dynamic model was verified using an experimental setup similar to that used for the static model verification. An accelerometer was placed on the suspended mass. For the first part of the verification, a constant air-mass system was tested. This provided a means to determine the damping constants, without using the valve model. The second part of the verification incorporated the valve model.

The constant mass tests were executed by inflating the actuator to a nominal pressure, and closing the valve. Then, the mass was given an initial displacement and released. To determine the damping constants it was assumed that the damping had two components, viscous and Coulomb. Equation (24) defines the relationship between the decrease in amplitude over one period and the damping components [13].

$$\Delta x = 4 \frac{\mu N}{k} + X \left(1 - \frac{1}{e^{\zeta \omega_n T_d}} \right) \quad (24)$$

where Δx = change in amplitude over one period, X = initial amplitude, ζ = damping ratio, ω_n = natural frequency, T_d = damped period. There is one equation and two unknowns. The two damping constants can be solved by measuring the change in amplitude at the beginning of the oscillation, and then again later in the waveform. The equations can then be solved simultaneously. Equation (24) can be expressed in terms of the damping constants for each measurement point.

$$\Delta x_1 = 4Q + X_1(1-b) \quad (25)$$

$$\Delta x_2 = 4Q + X_2(1-b) \quad (26)$$

Subtracting (26) from (25) and solving for b :

$$b = 1 - \frac{\Delta x_1 - \Delta x_2}{X_1 - X_2} \quad (27)$$

Solving (25) for Q considering b as known:

$$Q = \frac{\Delta x_1 - X_1(1-b)}{4} \quad (28)$$

This method was applied to solve for the damping constants. The viscous damping constant c is a function of the damping constant b from above.

$$c = 2\zeta m \omega_n \quad \text{and} \quad b = \frac{1}{e^{\zeta \omega_n T_d}} \quad (29, 30)$$

$$c = \frac{2m}{T_d} \ln\left(\frac{1}{b}\right) \quad (31)$$

The Coulomb and viscous damping are combined into an equivalent damping ratio, ζ_{eq} , which is given by the following relationship [12]:

$$\zeta_{eq} = \frac{\ln\left(\frac{X}{X - \Delta x}\right)}{2\pi} \quad (32)$$

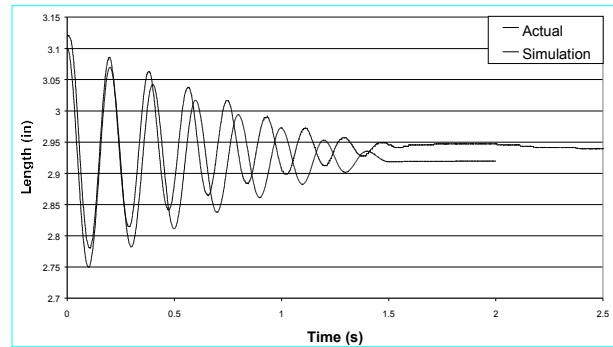


Figure 8: Comparison plot of actuator length vs. time for 60 psi nominal pressure and 6 lb suspended mass

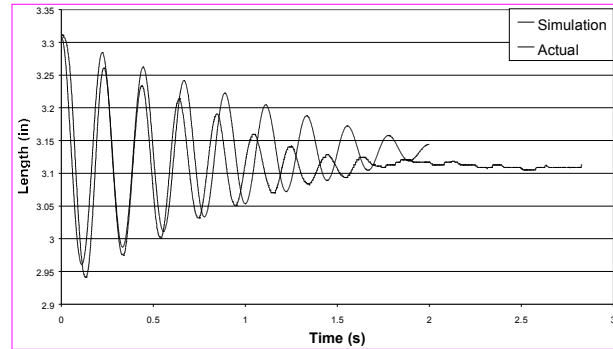


Figure 9: Comparison plot of actuator length vs. time for 80 psi nominal pressure and 11 lb suspended mass

The average damping constants determined by the above empirical analysis are:

$$Q = \frac{\mu N}{k} = 0.0044 \text{ in}, \quad c = 0.02 \text{ lb-s/in}, \quad \zeta = 0.035$$

These values were entered into the model, and the output of the simulation was compared to the empirical data in Figs. 8 and 9.

The natural frequencies are in good agreement, which validates the stiffness model. On the other hand, the model is less damped than the experiment when the 11lb load is used, independent of the nominal pressure. With the current damping model, no amount of tuning will cause agreement in all cases. This suggests that the damping may not be a constant. Note that even though the damping model is in error, the model has less damping and, therefore is better for control studies because instabilities will not be wrongly dissipated in the model.

Next we tested the valve model. A three-way solenoid valve was used to energize the actuator. It was opened and closed using PWM at 25 or 50 Hz and at a 50% duty cycle. Testing revealed that the valve opens in approximately 4 ms, and it closes in approximately 1 ms [10]. This means that any duty cycle that commands the valve to be open less than 4 ms will not open the valve. Also, any duty cycle that does not allow at least 1 ms for closing will never fully close the valve.

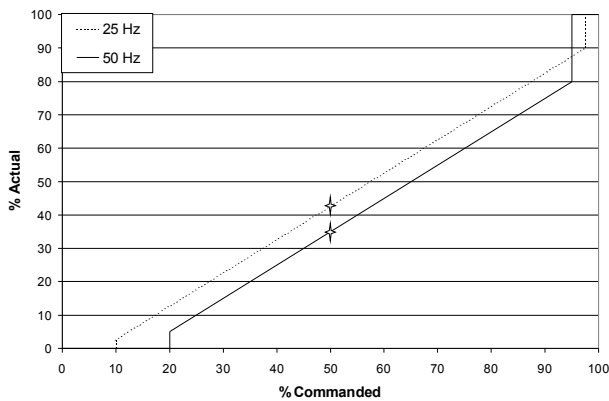


Figure 10: Relationship between the commanded and actual duty cycles.

A commanded duty cycle of 50% caused an actual duty cycle of 43% for 25 Hz and 35% for 50 Hz (Fig. 10). Therefore, the PWM duty cycle was adjusted in the simulation to match these values. For the output of the simulation, a correction factor or efficiency term was added to the valve model mass flowrate equation (21). This efficiency was set at 85% in all the simulation plots above. Plots of length versus time are shown in Figs. 11-13 for actual and simulated results.

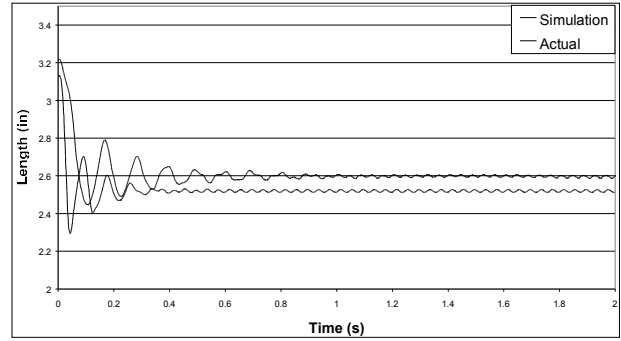


Figure 11: Actuator length vs. time for a 100 psi, 25 Hz, 1 lb system.

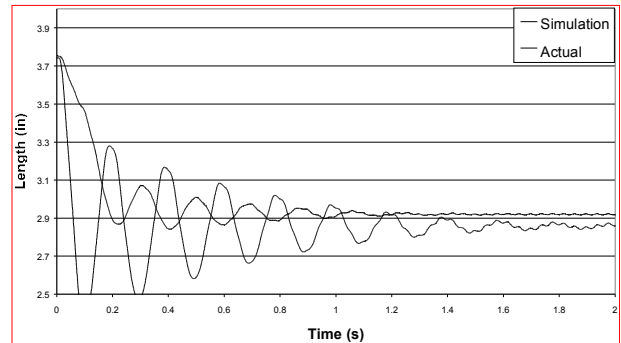


Figure 12: Actuator length vs. time for a 100 psi, 25 Hz, 5 lb system.

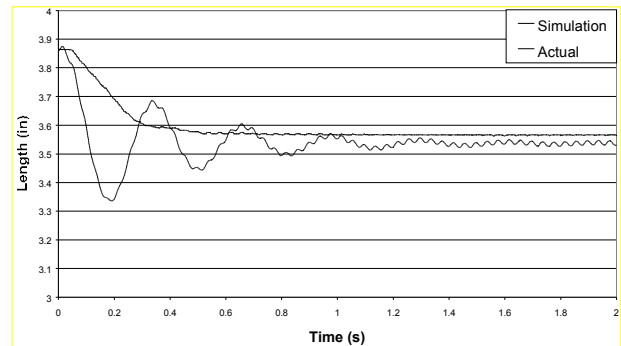


Figure 13: Actuator length vs. time for a 100 psi, 25 Hz, 15 lb system.

The results for a nominal PWM frequency of 50Hz are similar except the high frequency vibration is of a lower magnitude. These plots show that the valve model is adequate. Once again it is evident that the damping in the model is less than in the hardware. As the suspended mass M was increased, the steady state actuator length error decreased. This suggests that a better flow rate efficiency coefficient could have been chosen. The need for this efficiency factor and the under-damped waveforms may be attributed to the hoses or the valve model. The viscous losses that occur when the air flows through the plumbing

are not modeled in the system. If they were modeled, then there would be more damping, and also the mass flowrate into the actuator would decrease. A hose loss model could improve the dynamic actuator/valve model. However, we have found that the current model is sufficient for robot simulations and robot control.

4. Conclusions

Static and dynamic models of braided pneumatic actuators were presented. An adequate model of a solenoid valve working in conjunction with an actuator for use in robotic simulations was also presented. A modular actuator is invaluable for simulation and control. The input to the model is valve state, and the output is the force that the actuator produces. These models can aid in making versatile and accurate simulations of robots locomoting with BPA working in conjunction with solenoid valves. The usefulness of these models extends beyond large-scale biorobots such as Robot III [11]. The simulation can be tailored to fit any size actuator. In fact, the models are being used in design and control of a three inch long robot [1].

Acknowledgements

The Office of Naval Research N0014-99-1-0378 and DARPA DAAN02-98-C-4027 supported this work.

References

- [1] Birch, M.C., Quinn, R.D., Hahm, G., Phillips, S., Drennan, B., Fife, A., Verma, H., Beer, R.D. (2000) Design of a cricket microrobot. IEEE Conf. on Robotics and Automation, San Francisco, CA.
- [2] Caldwell, D.G., Medrano-Cerda, G.A., and Goodwin, M.J. (1995) Control of Pneumatic Muscle Actuators. *IEEE Control Systems Journal*, 15(1):40-48.
- [3] Chou, C.P., Hannaford, B. (1996) Measurement and Modeling of McKibben Pneumatic Artificial Muscles. *IEEE Transactions on Robotics and Automation*, 12(1):90-102.
- [4] Colbrunn, R. (2000) Design and Control of a Robotic Leg with Braided Pneumatic Actuators, M.S. Thesis, Case Western Reserve University, Cleveland OH.
- [5] Gaylord, R.H., Fluid actuated motor system and stroking device. U.S. Patent 2,844,126, July 22, 1958.
- [6] Inoue K. (1987) Rubbertuators and Applications for Robots. Proceedings of the 4th Symposium on Robotics Research, Tokyo, 57-63.
- [7] Klute, G.K., Czerniecki, J.M., and Hannaford, B. (1999) McKibben Artificial Muscles: Pneumatic Actuators with Biomechanical Intelligence, Proc. of the IEEE/ASME 1999 Int. Conf. on Advanced Intelligent Mechatronics, Atlanta, GA.
- [8] Klute, G.K and Hannaford, B. (1999) Modeling Pneumatic McKibben Artificial Muscle Actuators: Approaches and Experimental Results. ASME Journal of Dynamic Systems, Measurements, and Control.
- [9] McCloy, D. and Martin H.R. (1980) *Control of Fluid Power: Analysis and Design 2nd (revised) Edition*, Ellis Horwood Limited, New York.
- [10] Nelson G.M., (in press) Simulation and Control of a Cockroach-Like Robot, Ph.D. Thesis, Case Western Reserve University, Cleveland OH.
- [11] Nelson, G. M. and Quinn, R. D. (1999) Posture Control of a Cockroach-like Robot. *IEEE Control Systems*, 19(2).
- [12] Nickel, V.L., Perry, J. and Garrett, A.L. (1963) Development of useful function in the severely paralyzed hand. *Journal of Bone and Joint Surgery*, 45A(5):933-952.
- [13] Rao, S.S. (1955) *Mechanical Vibrations 3rd Edition*, Addison-Wesley, USA.
- [14] Shadow Robot Company (2000). <http://www.shadow.org.uk/products/airmuscles.shtml>
- [15] Tondu B., Boitier, V., and Lopez, P. (1994) Naturally Compliant Robot-arms Actuated by McKibben Artificial Muscles. Proceedings of the 1994 IEEE Int. Conf. on Systems, Man and Cybernetics, San Antonio, TX, 3:2635-2640.
- [16] Ye, N., Scavarda, S., Betemps, M., Jutard, A. (1992) Models of Pneumatic PWM Solenoid Valve for Engineering Applications, *Journal of Dynamic Systems Measurement and Control, Transactions of the ASME*, 114:680-688.